Trans Indian Inst Met (2024) 77(2):477–483
https://doi.org/10.1007/s12666-023-03137-3

ORIGINAL ARTICLE

Creep Behavior of Ultrasonically Processed AZ91/Nano-Alumina Composites

Nikita Goel[1] · Neeraj Srivastava[1,2] · Gajanan P. Chaudhari[1]

Received: 26 May 2023 / Accepted: 25 September 2023 / Published online: 17 October 2023

Abstract Mechanical properties of metal matrix nanocomposites mainly depend on the distribution, size, and inter-particle spacing of nanoparticles in the matrix. AZ91 alloy nanocomposites are fabricated by adding 0%, 0.5%, 1%, and 3% by weight of 50 nm size Al_2O_3 particles assisted by ultrasonic solidification technique. The grain size and particle distribution of nanocomposites are quantitatively studied using optical and scanning electron microscopy. Less agglomeration and better distribution of nano-sized particles are observed even up to 3 wt% addition. Indentation creep tests are performed on the as-cast base alloy and prepared nanocomposites at a temperature of 498 K using three different applied stresses of 222 MPa, 305 MPa and 388 MPa. Better distribution of alumina nanoparticles resulted in significant increase in the tensile strength and creep resistance of nanocomposites over that of the as-cast alloy. AZ91/3 wt% alumina composite exhibited the highest creep resistance.

Keywords Creep · Magnesium · MMC · Ultrasonication

1 Introduction

Magnesium alloys are candidate materials for structural materials in automobile, aviation and other fields when weight reduction is desired without compromising overall strength. Mg is the lightest metal that is 75% lighter than steel and 33% lighter than aluminum [1]. Despite their low density, Mg alloys have comparable strength-to-weight ratios [2, 3]. They are slowly replacing aluminum alloys and steels in some aerospace, electronics, and automotive applications [4, 5]. The most widely used AZ91 (Mg–9 wt %Al–0.8 wt%Zn–0.2 wt%Mn) alloy has many energy saving applications due to its light weight, better corrosion resistance, good dimensional stability, extremely good castability, and superior strength as compared to other magnesium alloys [5, 6]. However, it has tendency for oxidation, possesses lower strength and exhibits poor creep resistance [7]. Applications of AZ91 alloy are limited due to the presence of a low melting point (437 °C) $Mg_{17}Al_{12}$ phase, which also dissolves in the matrix above 130 °C and adversely affects the creep resistance [5, 7].

In order to enhance the strength and creep resistance of AZ91 alloy, a more effective method could be dispersion strengthening by adding micron and nano-sized hard particles [8, 9]. Reinforcing of Mg alloys using micron and nano-sized particles such as SiC [9], Al_2O_3 [9], carbon nanotube[10], carbon black[11], nano-graphene oxide[12], AlN[13], TiO_2[14], TiC[15], and TiB_2[16] is widely investigated. Lan et al. [17] investigated the effect of ultrasonic treatment (UST) on distribution of nano-silicon carbide particles in AZ91 alloy and reduced clustering of particles is reported in comparison with composites fabricated by conventional stirring process, which led to higher hardness of the composites. The strength of AZ91D/1 wt% of 25 nm AlN composite synthesized

Nikita Goel, Neeraj Srivastava have equally contributed.

✉ Gajanan P. Chaudhari
g.chaudhari@mt.iitr.ac.in

Neeraj Srivastava
neeraj.s@med.svnit.ac.in; neerajajai@gmail.com

[1] Department of Metallurgical and Materials Engineering, Indian Institute of Technology, Roorkee 247667, India

[2] Present Address: Department of Mechanical Engineering, Sardar Vallabhbhai National Institute of Technology, Surat 395007, India

by Cao et al. [13] using UST was improved significantly while ductility was retained. Khandelwal et al. [4] added nano-sized alumina particles in AZ31 alloy and reported significant increment in tensile strength and ductility of composites, which is attributed to thermal mismatch and Orowan strengthening mechanisms. Paramsothy et al.[6] investigated the effect of nano-Si_3N_4 particles on AZ31 and AZ91 alloy nanocomposites. These nanoparticles increased the tensile failure strain of composites. Fang et al. fabricated the AZ31 alloy nanocomposites and reported that TiB_2 particles refined the grain size of primary phase and led to an improvement in strength and ductility [18]. Nie et al. fabricated SiC/AZ91 alloy nanocomposites using semisolid stirring followed by UST [9]. Muley et al. fabricated the ultrasonically treated AZ91 alloy in situ composites [2]. Formation of in situ Mg_2Si phase improved the mechanical and wear resistance properties of composites.

Ceramic-reinforced MMCs are fabricated by various techniques such as stir casting [19], infiltration method [1], squeeze casting [20], powder metallurgy [21], and equal channel angular pressing [22]. Among these methods, mechanical stirring is an economical and commonly used method. However, nano-sized particles form clusters in the melt during mechanical stirring due to their higher surface energy [23]. Therefore, employing ultrasonic vibrations in the melt could be an alternate, simple and effective physical method that could break the agglomerates and distribute the nanoparticles uniformly throughout the melt [23]. Because nanocomposites fabricated by UST have potential to produce uniform distribution of reinforcing, hard, nano-sized particles [24], it is interesting to study their mechanical behavior.

Among above-mentioned ceramic particles, Al_2O_3 particles have been selected due to their high temperature strength and stability [25]. In addition, there is reasonable difference between the thermal expansion coefficients of α-Mg (26.1×10^{-6}/K) and alumina (7.4×10^{-6}/K) [4], which could result in great amount of dislocation density during cooling which may also be helpful for increasing the mechanical properties of AZ91 alloy. Therefore, in the present research work, the efficacy of UST on the distribution, inter-particle spacing, and size of nano-sized alumina clusters in AZ91 is studied using optical microscopy (OM) and scanning electron microscopy (SEM). Tensile and creep properties of as-cast alloy and its nanocomposites are investigated. Creep resistance is measured using indentation creep tests done at 225 °C.

2 Materials and Methods

Commercial AZ91 magnesium alloy procured from Exclusive Magnesium, Hyderabad, India, was used as a base alloy for nanocomposite production. The alloy chemical composition is given in Table 1 [26].

Reinforcing alumina particles had an average particle size of 50 nm. To fabricate magnesium alloy composites reinforced with nano-γ-alumina, mechanical stirring of the melt was followed by ultrasonic treatment (UST). A 1.5 kW ultrasonic processing unit (Model VCX 1500 from Sonics and Materials, USA) with 20 kHz frequency was integrated with an ultrasonic probe made of coated Ti-6Al-4 V alloy and a piezoelectric lead zirconate titanate air cooled converter crystal. Vibration amplitude of 60 µm used in UST was same for each casting. The experimental setup is described in an earlier work [26].

Nanocomposites with 0.5, 1, and 3 wt% alumina were fabricated. For each casting, 250 g of AZ91 alloy was melted in a mild steel crucible by heating it to 700 °C. The equilibrium liquidus and solidus temperatures of the AZ91 alloy are 598 °C and 468 °C [27]. A thermocouple was positioned in the molten metal to monitor the temperature throughout the experiment. Nano-sized alumina particles wrapped in aluminum foil were preheated at a temperature of 400 °C for 15 min and added in to the melt with the help of plunger. Then, the melt was stirred mechanically for about 600 s. UST of the melt was done by dipping preheated ultrasonic probe into melt for 180 s. A coating of zirconia was applied on the probe to prevent sticking of the melt. Thereafter, the melt in the mild steel crucible was air cooled. For comparison, an as-cast control specimen was prepared similarly without addition of alumina.

The samples for microstructural analysis were obtained from the middle of the casting after sectioning. These were prepared by polishing using SiC paper followed by cloth polishing using diamond paste. Then, the samples were ultrasonically cleaned and etched with acetic picral solution for 3–5 s. The microstructural analysis was done using a Leica DMI 5000 M optical microscope. Distribution of nano-sized particles was observed in ultrasonically cleaned samples using a Zeiss MA18 scanning electron microscope (SEM). Hardness tests were done using FIE-VM50PC Vickers hardness tester with a load of 1 kg and dwell time of 10 s. For each sample, test was repeated five times and mean value has been reported. Using a strain rate of 10^{-3} s^{-1}, the tensile properties were determined by using a 25 kN Tinius Olsen machine. For each alloy/ composite, minimum three tensile samples were tested. Creep tests were carried out using a Spranktronics® indentation creep machine. For the creep experiments, samples of

Table 1 Chemical composition of AZ91 alloy

Elements	Mg	Al	Zinc	Mn	Si	Cu	Ni	Fe
Contents (mass %)	Balance	9.30	0.71	0.21	0.10	0.03	0.005	0.002

size 15 mm × 15 mm × 7 mm were sectioned from the middle of each casting using a low-speed diamond saw. In creep test, tungsten carbide indenter of 1.5 mm diameter was impressed against the sample surface using specific loads corresponding to stress of 222 MPa, 305 MPa and 388 MPa. Indentation creep tests were performed at 225 °C for up to 10^5 s. In order to prevent the oxidation of creep samples, tests were performed under a vacuum of 10^{-7} Pa.

3 Results and Discussion

3.1 Microstructural Analysis

Figure 1 shows the optical micrographs of as-cast AZ91 alloy and its nanocomposites. The phases present include α-Mg matrix, and β-$Mg_{17}Al_{12}$ phase. Figure 1a shows the relatively coarse dendritic structure of as-cast alloy. By increasing the amount of nano-alumina, higher degree of refinement in grain size is observed in nanocomposites (Fig. 1b–d). Relative grain sizes of AZ91 alloy and its nanocomposites are summarized in Table 2. The amount of added nanoparticles influence the average grain size of primary phase in the resulting nanocomposites. The grain sizes of all the nanocomposites are smaller than that of the base alloy. Upon adding 0.5 wt% of nano-alumina particles accompanied with ultrasonic processing, the average grain size is reduced from 245 µm for the base alloy to 217 µm, i.e., by about 11% (Fig. 1 and Table 2). Similarly, addition of 1 wt% and 3 wt% of nano-alumina particles to the base alloy reduces the average grain size by 17% and 21%, respectively. For 3 wt% of alumina composites, the coarse dendritic structure of base alloy is changed to very fine dendritic structure. UST successfully limits the agglomeration of alumina nanoparticles, resulting in an average agglomerate size of 70, 100, and 170 nm for the 0.5, 1, and 3 wt% of alumina added composites. Reduction in grain size is clearly due to reinforcing nano-sized Al_2O_3 particles that act as active

Table 2 Grain size variation with respect to content of reinforcement

Reinforcement, wt%	0	0.5	1	3
Average grain size of α-Mg, µm	245 ± 15	217 ± 7	202 ± 7	187 ± 8
Particle/agglomerate size, nm	–	70 ± 5	100 ± 8	170 ± 22

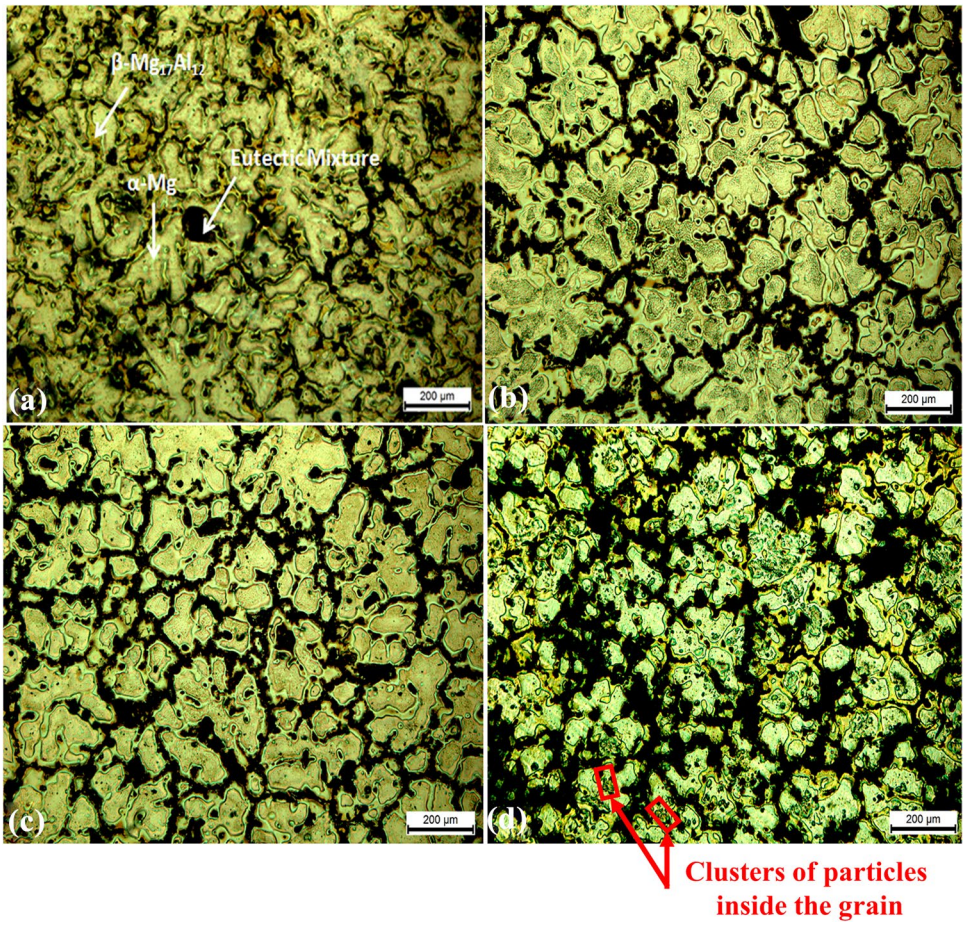

Fig. 1 Optical images of **a** as-cast AZ91 alloy, **b** AZ91/0.5 wt% Al_2O_3 **c** AZ91/1 wt% Al_2O_3 and **d** AZ91/3 wt% Al_2O_3 nanocomposites

nucleation sites. By increasing the content of nano-sized particles, grain size of nanocomposites progressively decreases due to increasing number of heterogeneous nucleation sites. Thermal properties of liquid melt and reinforced particles are important for particles to act as heterogeneous nucleation sites for primary phase [28–30]. For particles acting as a heterogeneous nucleation site during solidification, the specific heat capacity and thermal diffusivity of particles should be smaller than that of the liquid melt. Specific heat capacity of AZ91 alloy and alumina is 1.05 kJ kg^{-1} K^{-1} [31] and 0.88 kJ kg^{-1} K^{-1} [32], respectively. Due to lower specific heat capacity of alumina particles, alumina particles will be locally undercooled than liquid magnesium during solidification and act as nucleation sites for α-Mg grains. This could also be the reason why alumina particles are detected inside the grains (Fig. 1d).

Figure 2 shows SEM micrographs of all the nanocomposites. For AZ91-0.5 wt% alumina composites, a better dispersion of nano-sized Al_2O_3 particles with fewer sites of nanoparticle agglomeration in the α-Mg matrix is visible in Fig. 2a. Upon adding 2 wt% of alumina, higher amount of single nano-sized particles and some clusters of nanoparticles are observed in Fig. 2b. Addition of 3 wt% of particles results in higher fraction of particle agglomerates. This is due to increase in the viscosity of the melt, reducing the efficiency of UST in breaking and dispersing of nano-sized particles. Yet, the distribution of alumina particles/agglomerates in Fig. 2c is also even. Mechanisms of dispersion of nano-sized particles is discussed in detail earlier [4, 33]. The inter-particle distance decreases from 730 nm for 0.5 wt% alumina to 460 nm for 1 wt% alumina and to 150 nm for 3 wt% alumina particles. There is 37% decrease in inter-particle spacing for 1 wt% alumina and ~ 80% for 3 wt% alumina as compared to 0.5 wt% alumina. This can enhance the mechanical properties of nanocomposites by increase in the yield strength due to increased contribution from Orowan and thermal mismatch strengthening [26].

3.2 Mechanical Properties

Figure 3 shows the hardness of processed nanocomposites as a function of nano-alumina content. Hardness of different fabricated nanocomposites is greater than that of AZ91 alloy and it increases almost monotonously with the alumina content. Nano-sized alumina particles hinder the movement of

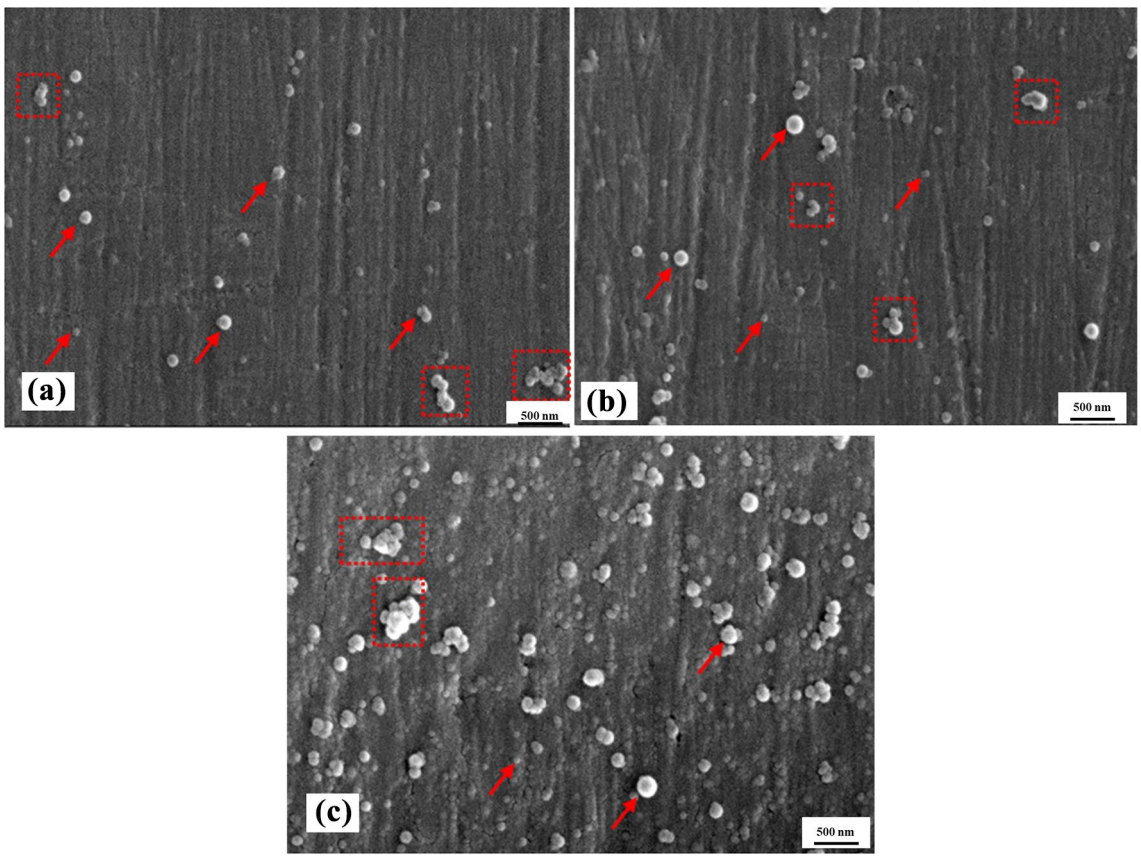

Fig. 2 SEM micrographs of **a** AZ91/0.5 wt% Al_2O_3 **b** AZ91/1 wt% Al_2O_3, and **c** AZ91/3 wt% Al_2O_3 nanocomposites. Arrows and dotted rectangles show single particle and clusters of nano-particles, respectively

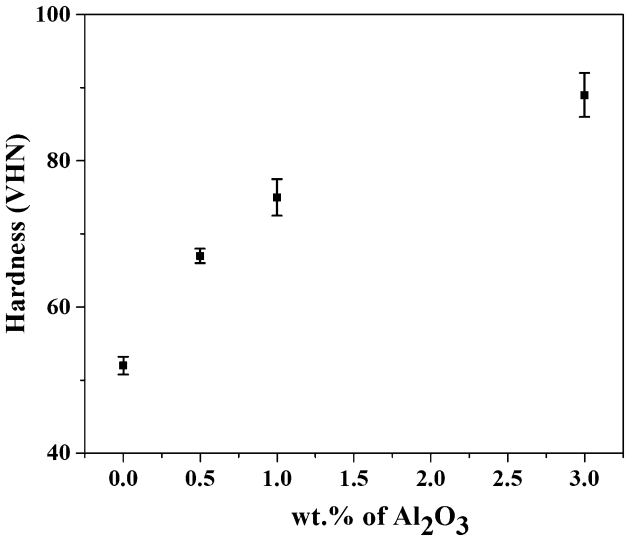

Fig. 3 Hardness of AZ91 alloy and processed nanocomposites

dislocations, thus strengthening it and leading to the increase in hardness.

Figure 4 depicts the engineering stress–engineering strain curves of the base alloy and nanocomposites, and Table 3 summarizes the tensile properties. There is enhancement of tensile properties of all nanocomposites as compared to the base alloy. All the nanocomposites show yield strength values higher than that of the base alloy, with the yield strength of 3 wt% Al_2O_3 composite being the highest followed by 2 wt% Al_2O_3 composite, and 0.5 wt% alumina composite. It can be observed that AZ91/3 wt% Al_2O_3 shows the best combination of strength and ductility. There is an enhancement of total elongation from about 2% for as-cast AZ91 alloy to 3% for AZ91/3 wt% Al_2O_3 composite. Enhancement in ductility for AZ91-nano-alumina composites occurs

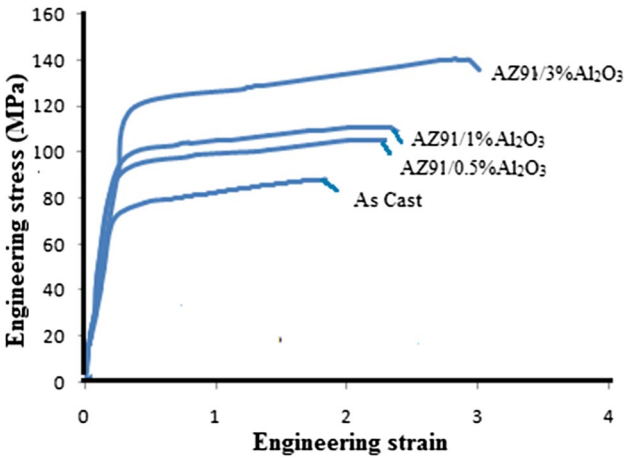

Fig. 4 Engineering stress–strain curves of AZ91 alloy and its nanocomposites

Table 3 Mechanical properties of AZ91 alloy and its nanocomposites

Material	Yield strength (MPa)	Ultimate tensile strength (MPa)	Elongation (%)
AZ91 alloy	75	88	2
AZ91/0.5 wt% Al_2O_3	90	106	2.4
AZ91/1 wt% Al_2O_3	97	110	2.4
AZ91/3 wt% Al_2O_3	120	140	2.9

from effective resistance to the crack propagation during deformation due to uniform dispersion of nanoparticles [4]. Thus, the nanocomposites exhibit higher yield strength, tensile strength and % elongation values, suggesting higher tensile toughness as reflected in their larger area under the stress–strain curves, as compared to the base alloy. Direct and indirect strengthening mechanisms are responsible for improved mechanical properties of ex situ magnesium composites [4]. Direct strengthening occurs due to effective load transfer from matrix to reinforcement as a consequence of uniform dispersion and higher content of nano-alumina particles. Indirect strengthening occurs because of thermal mismatch between the AZ91 alloy (26.1×10^{-6}/K) and alumina particles (7.4×10^{-6}/K) resulting in an increase in dislocation density during cooling, called as thermal mismatch strengthening. Indirect strengthening also occurs from Orowan strengthening mechanism. It occurs due to Orowan looping by nano-alumina particles which act as a pinning point for dislocations. Better nanoparticles dispersion effectively contributes to Orowan strengthening and thermal mismatch strengthening, which works as major factors in increasing the strength of nanocomposites.

Figures 5 shows creep curves for different AZ91/nano-alumina composites tested for up to 11000 s at a temperature of 225 °C using different applied stress. Primary creep region is followed by secondary creep. There is a decrease in creep rate with time during the primary creep as dislocation density increases due to which material gets work hardened. However, balance between rate of work hardening and rate of recovery sets in during secondary creep, making the creep rate nearly constant. The minimum creep rate, $\dot{\varepsilon}$, observed during secondary creep is expressed by Eq. 1[34].

$$\dot{\varepsilon} = \frac{\partial h}{\partial t} \tag{1}$$

where 'h' and 't' denote depth of indentation in mm and time in s, respectively. The nature of indentation creep precludes tertiary creep and fracture of samples.

Creep curves show that the creep resistance of the AZ91 alloys is enhanced by the addition of nano-Al_2O_3 particles. Increasing the applied stress from 222 to 388 MPa results in a higher penetration depth. The indentation creep curves

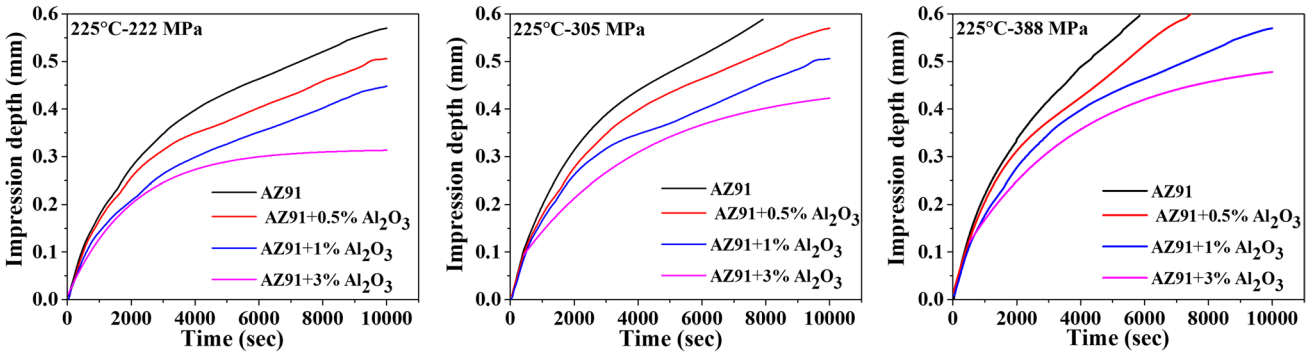

Fig. 5 Creep behavior of AZ91 alloy and its nanocomposites

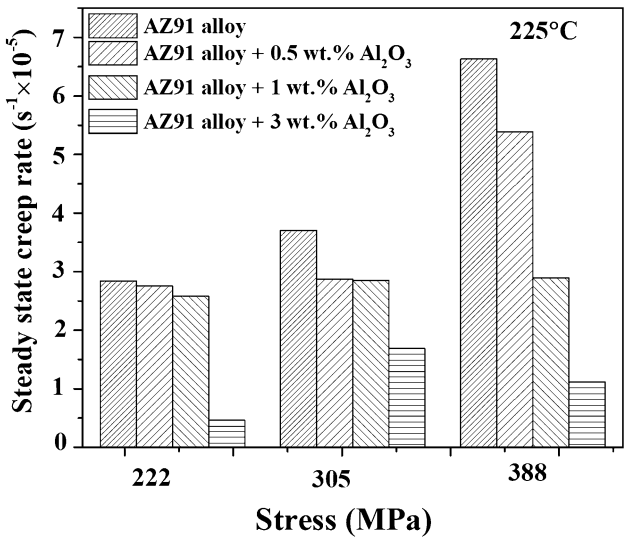

Fig. 6 Steady-state creep rate of AZ91 alloy and its nanocomposites

at temperature of 225 °C under constant stress at 222 MPa show that depth of indentation decreases with increase in nano-Al_2O_3 content of the composites. At all applied stress values, AZ91 alloy shows the highest penetration depth followed by AZ91/0.5% nano-alumina composite. The depth of indentation is lowest for AZ91/3 wt% nano-alumina composite. Similar trend in creep behavior is seen at higher stress levels of 305 and 388 MPa.

The steady-state creep rates of the AZ91 alloy and its nanocomposites are shown in Fig. 6. It can be observed that the addition of nano-alumina significantly increases the creep resistance of AZ91 alloy. AZ91 base alloy has no role of Orowan and thermal mismatch strengthening to increase the creep resistance. On the other hand, steady-state creep rate is lowest for the nanocomposite with 3 wt% alumina. Here, Orowan strengthening and thermal mismatch strengthening contribute very effectively due to the presence of fewer and smaller agglomerates, and uniform distribution of nanoparticles. Table 2 shows that the average particle/agglomerate size for 3 wt% alumina composite is 170 nm. Whereas some particle agglomerates with the size of 200–500 nm are still observed, remaining particles/agglomerates with < 100 nm size plays a very important role in enhancing the creep resistance. In addition, the presence of nano-alumina particles within the grains and in the grain boundary region inhibits the motion of dislocations as well as restrict grain boundary sliding during creep deformation which enhances the creep resistance of nanocomposites.

4 Conclusions

Mechanical and creep behavior of ultrasonically processed AZ91-nano-alumina composites has been studied. Different nanocomposites were produced by varying the amount of nano-sized alumina powder and processed by using ultrasound-assisted casting. Microstructure characterization, mechanical, and indentation creep tests were carried out. Major conclusions are:

(a) Ultrasonic treatment resulted in less agglomeration and more uniform dispersion of nano-sized alumina particles in all the nanocomposites.
(b) Agglomeration of nanoparticles present inside the nanocomposites increased with the amount of particles.
(c) Room temperature hardness and tensile strength of nanocomposites increased due to incorporation of hard alumina particles that retarded the movement of dislocations and thus increased the strength.
(d) Creep resistance of AZ91 alloy increased upon addition of nano-alumina particles, with 3 wt% Al_2O_3 composites showing the best creep resistance among the investigated composites due to less agglomeration and better distribution of alumina particles from ultrasonic treatment.

Acknowledgements Department of Science and Technology, Ministry of Science and Technology, Government of India (Grant no. SR/S3/ME/0024/2007) is acknowledged for financial support.

Declarations

Conflict of interest The authors report that there are no competing interests to declare.

References

1. Rani D, Rangaraj L, Suresha B, and Venkateswarlu K, *Transactions of the Indian Institute of Metals* **74** (2021) 743. https://doi.org/10.1007/s12666-021-02185-x
2. Muley S V, Singh S P, Sinha P, Bhingole P P, and Chaudhari G P, *Materials and Design* **53** (2014) 475. https://doi.org/10.1016/j.matdes.2013.07.056
3. Sen M, and Puri A B, *Materials Today Communications* **33** (2022) 105017. https://doi.org/10.1016/j.mtcomm.2022.105017
4. Khandelwal A, Mani K, Srivastava N, Gupta R, and Chaudhari G P, *Composites Part B: Engineering* **123** (2017) 64. https://doi.org/10.1016/j.compositesb.2017.05.007
5. Kabirian F, and Mahmudi R, *Metallurgical and Materials Transactions A: Physical Metallurgy and Materials Science* **40** (2009) 2190. https://doi.org/10.1007/s11661-009-9905-2
6. Paramsothy M, Chan J, Kwok R, and Gupta M, *Materials Science and Engineering A* **528** (2011) 6545. https://doi.org/10.1016/j.msea.2011.05.003
7. Guangyin Y, Yangshan S, and Wenjiang D, *Materials Science and Engineering A* **308** (2001) 38. https://doi.org/10.1016/S0921-5093(00)02043-8
8. Jayalakshmi S, Sahu S, Sankaranarayanan S, Gupta S, and Gupta M, *Materials and Design* **53** (2014) 849. https://doi.org/10.1016/j.matdes.2013.07.022
9. Nie K B, Wang X J, Wu K, Hu X S, and Zheng M Y, *Materials Science and Engineering A* **540** (2012) 123. https://doi.org/10.1016/j.msea.2012.01.112
10. Abbas A, Huang S J, Ballóková B, and Sülleiová K, *Tribology International* (2020). https://doi.org/10.1016/j.triboint.2019.105982
11. Bhingole P P, and Chaudhari G P, *Materials Science and Engineering A* **556** (2012) 954. https://doi.org/10.1016/j.msea.2012.07.104
12. Kumar P, Mallick A, Kujur M S, Tun K S, and Gupta M, *Materials and Manufacturing Processes* **35** (2020) 1650. https://doi.org/10.1080/10426914.2020.1784927
13. Cao G, Choi H, Oportus J, Konishi H, and Li X, *Materials Science and Engineering A* **494** (2008) 127. https://doi.org/10.1016/j.msea.2008.04.070
14. Song Y L, Sun X Y, and Liu Y H, *Materials and Corrosion* **63** (2012) 813. https://doi.org/10.1002/maco.201106251
15. Ferreira V, Merchán M, Egizabal P, et al., *Journal of Materials Research and Technology* **8** (2019) 2549. https://doi.org/10.1016/j.jmrt.2019.02.012
16. Xiao P, Gao Y, Yang C, Liu Z, Li Y, and Xu F, *Materials Science and Engineering A* **2018** (2017) 251. https://doi.org/10.1016/j.msea.2017.10.107
17. Lan J, Yang Y, and Li X, *Materials Science and Engineering A* **386** (2004) 284. https://doi.org/10.1016/j.msea.2004.07.024
18. Fang C, Liu G, Hao H, and Zhang X, *Materials Science and Engineering A* **2017** (2016) 592. https://doi.org/10.1016/j.msea.2016.12.072
19. Hassan K H, and Ramadan D O, *Transactions of the Indian Institute of Metals* **76** (2023) 1625. https://doi.org/10.1007/s12666-023-02874-9
20. Purazrang K, Abachi P, and Kainer K U, *Composites* **25** (1994) 296. https://doi.org/10.1016/0010-4361(94)90222-4
21. Ram B, Deepak D, and Bala N, *Transactions of the Indian Institute of Metals* **72** (2019) 1313. https://doi.org/10.1007/s12666-019-01627-x
22. Huang S J, Subramani M, Borodianskiy K, Immanuel P N, and Chiang C C, *Materials Today Communications* **2023** (34), (2022) 104974. https://doi.org/10.1016/j.mtcomm.2022.104974
23. Srivastava N, and Chaudhari G P, *Materials Science and Engineering A* (2018). https://doi.org/10.1016/j.msea.2018.03.092
24. Soni S K, Manimaran D, Thomas S B, and Thomas B, *Materials Today Communications* **2023** (2022) 105222. https://doi.org/10.1016/j.mtcomm.2022.105222
25. Verma V, and Kumar B V M, *Materials and Manufacturing Processes* **32** (1), (2017) 21. https://doi.org/10.1080/10426914.2016.1198023
26. Yadav S D, Bhingole P P, Chaudhari G P, Nath S K, and Sommitsch C, *Key Engineering Materials* **651–653** (2015) 783. https://doi.org/10.4028/www.scientific.net/KEM.651-653.783
27. Sedighi O, Shabestari S G, and Yavari F, *Thermochimica Acta* **667** (2018) 165. https://doi.org/10.1016/j.tca.2018.07.021
28. Xi L, Gu D, Guo S, and Wang R, *Integrative Medicine Research* **9** (2020) 2611. https://doi.org/10.1016/j.jmrt.2020.04.059
29. Rohatgi P, and Asthana R, *The Journal of The Minerals, Metals & Materials Society* **43** (1991) 35.
30. Ye H A I Z H I, and Liu X Y, *Journal of Materials Science* **39** (2004) 6153.
31. Avedesian MM, Baker H. *ASM Specialty Handbook: Magnesium and Magnesium Alloys*. ASM International; 1999.
32. Michael Bauccio. *ASM Engineered Materials Reference Book*. Second Edi. ASM International, Materials Park, OH; 1994.
33. Srivastava N, and Chaudhari G P, *Journal of Crystal Growth* **532** (2020) 125415.
34. Gupta R, and Daniel B S S, *Materials Science and Engineering A* **733** (2018) 257.